Title
FISSION THROUGHOUT THE PERIODIC TABLE

Authors
Moretto, L. B.
Wozniak, G. J.

Publication Date
1989-04-01

Lawrence Berkeley Laboratory
UNIVERSITY OF CALIFORNIA

Presented at the ANS Conference on Fifty Years
with Nuclear Fission, Gaithersburg, MD,
April 26–28, 1989, and to be published
in the Proceedings

Fission throughout the Periodic Table

L.G. Moretto and G.J. Wozniak

April 1989

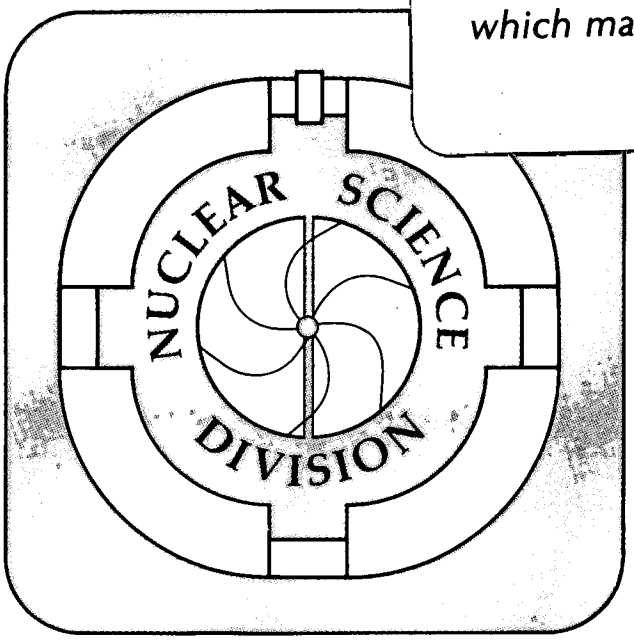

Prepared for the U.S. Department of Energy under Contract Number DE-AC03-76SF00098.

DISCLAIMER

FISSION THROUGHOUT THE PERIODIC TABLE

LUCIANO G. MORETTO and GORDON J. WOZNIAK
Nuclear Science Division, Lawrence Berkeley Laboratory,
1 Cyclotron Rd., Berkeley, California, 94720, USA

ABSTRACT

The dualistic view of fission and evaporation as two distinct compound nucleus processes is substituted with a unified view in which fission, complex fragment emission, and light particle evaporation are seen as different aspects of a single process.

I. INTRODUCTION

A. Early history and traditional views

The answer to the simple question "What is fission?" is not unique but depends upon the space and time cross section of the scientists to whom the question is addressed. Before 1939, fission was still in imaginary space. It soon emerged into an altogether too real world by virtue of two chemists who dared thinking the unthinkable. Even today many of our physics colleagues think of fission as a peculiar reaction occurring around uranium, a somewhat embarassing process that gave and still gives us a bad reputation; then with nuclear bombs, now with nuclear energy.

Even among "experts," fission is typically associated with heavy elements. If its presence is acknowledged, as far down as the Lead region and even lower, its existence becomes progressively more evanescent as one moves farther down the periodic table and its cross section becomes lost in the abyss of nanobarns. Most emphatically, fission is believed to be a unique kind of compound nucleus reaction when compared with the more commonplace decays, like those involving the emission of protons, alphas and other "particles." Fission appeared so different from the other modes of compound nucleus decay that a separate theory was devised to calculate its decay width. As a result, we now have one theory for "evaporation" and another for fission.

Yet, a typical mass distribution of fission fragments while peaked, at times sharply, at masses near the symmetric splitting, is nonetheless a continuous distribution for which there are no firm boundaries other than those set by the total mass of the system. In all fairness, the search for ever lighter (and heavier) fission products was actively pursued by radiochemists, who were eventually stopped only by the abysmally small cross sections. So the belief was consolidated that fission fragments were confined to a rather narrow range of masses, despite the occasional disturbing detection of intermediate mass or complex fragments like Na, Si, etc. in higher energy reactions.[1-4] With a curious twist of insight, these lighter fragments were at times attributed to ternary fission, rather than to a more obvious, highly asymmetric binary fission. But, why should the fission mass distribution not extend all the way to alpha particles and protons?

B. The turbulent history of complex fragments

The advent of low energy heavy ions familiarized the nuclear community with products of deep inelastic reactions ranging throughout the periodic table.[5-7] While, in many ways, deep inelastic reactions do remind us of fission, the obvious genetic relationship of these products with either target or projectile keeps these processes more or less within the categorical boundaries of "direct reactions."

Complex fragments made their grand entrance with intermediate-energy heavy ion reactions. In these processes, the elegant simplicity of quasi and deep inelastic processes is substituted by a glorious mess of products that seem to bear no relationship to either of the entrance channel partners. Their glaringly abundant production, together with the turbid experimental environment prevailing in early studies, prompted a tumultuous development of theories, claims and counterclaims about their origin and manner of production.

The broad mass range and abundance of these fragments suggested mechanisms like the shattering of glass-like nuclei[8] or the condensation of droplets out of a saturated nuclear vapor.[9-14]

Fortunately, in spite of the confusion, it did not escape some perceptive members of our community that most, if not all of the complex fragments were associated with essentially binary processes. Furthermore, after an allowance was made for target and projectile-like fragments, the remaining fragments appeared to originate from the binary decay of an isotropic source. Finally, the excitation functions of these fragments appeared to behave in accordance with compound nucleus branching ratios. The inescapable conclusion was that compound nucleus decay was responsible for the production of these fragments by a mechanism able to feed

all the possible asymmetries. Such a mechanism without undue strain of the imagination could be well identified with a generalized fission process.

C. Fission, fission everywhere.....

This evidence, which continues to grow by the day, demonstrates the very pervasive presence of statistical complex fragment emission throughout the periodic table, at low and high excitation energies, covering the entire range of asymmetries, though not with equal intensity. In fact, the observed modulation of the mass distribution is a most revealing signature of the underlying potential energy as a function of mass asymmetry and underscores the essential unity of these processes.

Here one has the key for the unification of all compound nucleus decays into a single process. The natural connection between all these modes of decay is the mass asymmetry coordinate. Typical light particle evaporation (n, p, alpha, etc.) corresponds to very *asymmetric* decays, while "fission" of heavy systems corresponds to a very *symmetric* decay. The lack of emission at intermediate asymmetries is only apparent. Such an emission does in fact occur, albeit very rarely at low energies. The rarity of this occurrence is due to the important but accidental fact of the high potential barriers associated with the emission. A suitable increase of the excitation energy, or the lowering of the barriers by an increase in the angular momentum, readily increases the cross section of these intermediate mass fragments to an easy level of detection.

Similarly the apparent lack of "fission" in lighter systems, suggested by the absence of a symmetric fission peak in the mass distribution, is another manifestation of the underlying potential energy that forces the mass distribution to assume a characteristic U shape. Consequently, in spite of the variety of mass distributions brought about by the different dependence of the potential energy on the mass asymmetry, we are confronted with a single process responsible for the production of the whole range of masses from the decay of compound nuclei throughout the periodic table (with the notable exception of gamma ray and meson emission). This process, with a minimal generalization of the term might well be called "fission."

In this way we have reached a very remarkable conclusion. Fission, rather than being a peculiar process relegated to the upper reaches of the periodic table and to a remote area of nuclear physics cultivated by oddball scientists, surprisingly turns out to be <u>the</u> most general, all-pervasive reaction in compound-nucleus physics. If anything, it is the standard evaporation that should be regarded as a peculiar limiting case of very asymmetric fission... Like the ghost of Hamlet's father, fission is "*hic et ubique* ," here, there and everywhere.

II. GENERALIZED FISSION THEORY

Particle evaporation traditionally includes neutron, proton and alpha particle emission. In its simplest form, the decay width is typically written down in terms of the inverse cross section and of the phase space of the system with the particle at infinity as:

$$\Gamma(\varepsilon)d\varepsilon = \frac{8\pi g m}{2\pi\rho(E)h^2}\,\varepsilon\sigma(\varepsilon)\,\rho(E-B-\varepsilon)d\varepsilon \qquad (1)$$

where $\rho(\varepsilon)$ and $\rho(E-B-\varepsilon)$ are the level densities of the compound nucleus and residual nucleus, respectively; m, ε, g are mass, kinetic energy and spin degeneracy of the emitted particle; and $\sigma(\varepsilon)$ is the inverse cross section.[15-18]

The fission decay width is commonly evaluated by following the Bohr-Wheeler formalism which makes use of the transition-state method. In this approach, the reaction (fission) coordinate is determined at a suitable point in coordinate space, (typically at the saddle point) and the decay rate is identified with the phase space flux across a hyperplane in phase space passing through the saddle point and perpendicular to the fission direction. The decay width is written[19] as:

$$\Gamma_f = \frac{1}{2\pi\rho(E)}\int\rho^*(E-B_f-\varepsilon)d\varepsilon, \qquad (2)$$

where $\rho(E)$ and $\rho^*(E-B_f-\varepsilon)$ are the level densities of the compound nucleus and of the saddle point; ε is the kinetic energy along the fission mode; and B_f is the fission barrier. So, the dichotomy between fission and evaporation is emphasized even in the expressions for the corresponding decay rates.

It was observed some time ago that this dichotomy is deceptive.[20,21] The separation between evaporation and fission, is an optical illusion due to the very low cross section of products with masses intermediate between ^{4}He and fission fragments. There is no need to consider the two extremes of this distribution as two independent processes. **Rather, fission and evaporation are the two, particularly (but accidentally) obvious extremes of a single statistical decay process, the connection being provided in a very natural way by the mass asymmetry coordinate.**

A. Potential energy, absolute and conditional saddle points, and ridge line

The potential-energy surface $V(\tilde{q})$ as a function of a set of deformation coordinates $\tilde{q}$ has been studied in detail first within the framework of the liquid-drop model,[22-24] and, more recently of the finite-range model.[25,26]

In general, only the stationary points of the potential-energy surface corresponding to the solutions of the above equation are of intrinsic physical significance. However, saddle-point shapes for fissility parameter values of $x < 0.7$ are strongly constricted at the neck, so that the nascent fission fragments are already well defined in mass, and a physical significance to the mass asymmetry parameter $A_1/(A_1 + A_2)$ can be assigned. Then it is possible to consider a cut in the potential energy along the

mass-asymmetry coordinate passing through the fission saddle point, with the property that at any point the potential energy is stationary with respect to all the other degrees of freedom. Each point is then a "conditional saddle point" with the constraint of a fixed mass asymmetry. This line has been called[20,21] the "ridge line" in analogy with the term "saddle point". The general shape of the ridge line depends on whether the fissility parameter lies above or below the Businaro-Gallone point.[27] The properties of the ridge line above and below the Businaro-Gallone point are illustrated in Fig. 1.

Below the Businaro-Gallone point, the ridge line shows a single maximum at symmetry. This is a saddle point of degree of instability two (the system is unstable both along the fission mode and the mass asymmetry mode). As the fissility parameter x increases above x_{BG}, this saddle point splits into three saddle points. The symmetric saddle point is stable with respect to the mass-asymmetry mode (degree of instability one) and is the ordinary fission saddle point. The other two saddles, of degree of instability two, are called Businaro-Gallone mountains, and flank symmetrically the fission saddle point.

The incorporation of angular momentum maintains essentially the same topology. Its main effect is to decrease the overall heights of the barriers and to displace the Businaro-Gallone point towards lower values of the fissility parameter.

B. Complex fragment radioactivity as a very asymmetric spontaneous fission decay.

The explicit introduction of the mass-asymmetry coordinate in the problem of complex fragment emission, resulting in the ridge line as a generalization of the fission saddle point, leads, as a first application, to the theory of complex fragment radioactivity. Let us consider the qualitative picture in Fig. 2 where the potential energy is shown as a function of the mass asymmetry coordinate as well as of the fission coordinate (decay coordinate). The ridge line divides the compound nucleus domain from the fission-fragment domain. A continuum of trajectories is available for the decay, from the easy path through the saddle point, to the very arduous path reaching up to the Businaro-Gallone mountains, and down to the progressively easier paths of more and more asymmetric decays, eventually leading to α-particle and nucleon decay.

For spontaneous decay we can associate each path with the action integral:

$$S(Z) = \int |p(x)|dx = \int_a^b [2\mu(Z)\, V(Z,x)]^{1/2} dx \qquad (3)$$

where $|p(x)|$ is the modulus of the momentum along the fission coordinate x; $\mu(Z)$ and $V(Z,x)$ are the inertia and the potential energy for each asymmetry Z; and **a** and **b** are the classical turning points of the trajectory. The decay rate P(Z) can be written, semiclassically, as:

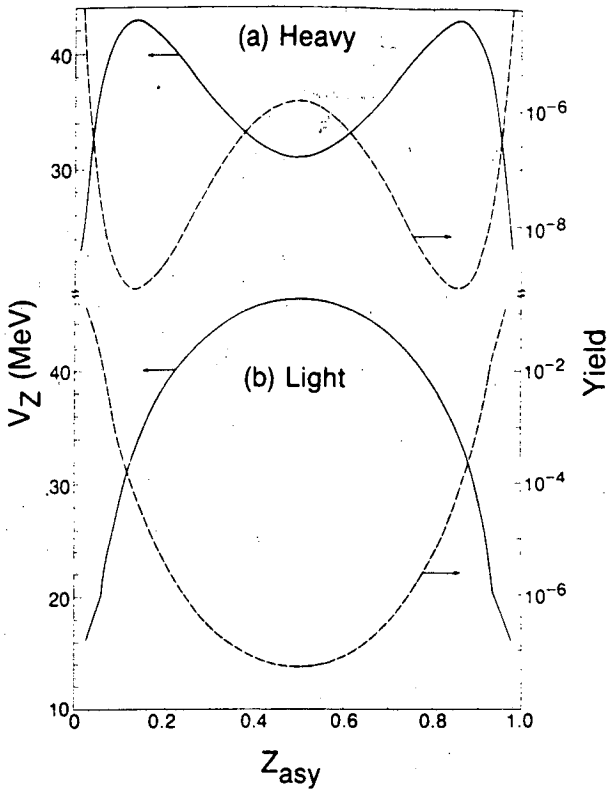

Fig. 1 Schematic ridge-line potentials (solid curve) and expected yields (dashed curve) for: a) a heavy CN above the Businaro-Gallone point; and b) a light CN below the Businaro-Gallone point as a function of the mass asymmetry coordinate (Z_{asy}). See Eq. 6 in the text.

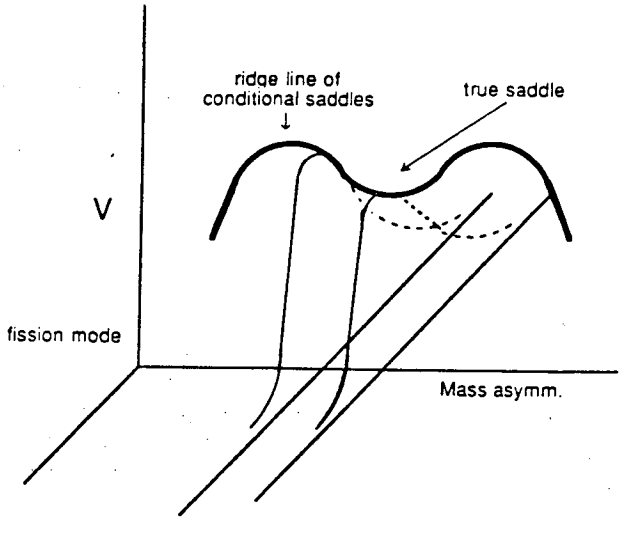

Fig. 2 Schematic potential energy surface as a function of the reaction coordinate and of the mass-asymmetry coordinate.

$$P(Z) = w(Z)\, \exp\left[\frac{-2S(Z)}{\hbar}\right] \qquad (4)$$

where w(Z) is the frequency of assault of the barrier for the asymmetry Z.

This simple expression accomodates the radioactive emission of any fragment, provided that the process is energetically possible. Of course the strong dependence of the decay rate on the barrier height tends to favor the emission of very light particles on the one hand, and, for very heavy elements, spontaneous fission decay. For light particle emission, shell effects play a dominant role. The strong magicity of ^{4}He accounts for the very pervasive α radioactive decay. The recently observed[28-31] radioactive emission of ^{14}C and ^{24}Ne can be accounted for in a very similar way by the very strong shell corrections associated with the residual nuclei in the ^{208}Pb region. Extensive discussions of this problem can be found in Refs 32, 33 &34.

C. Complex fragment decay width

The role of the ridge line on the emission of complex fragments can be appreciated by observing that for $x < 0.7$ at all asymmetries and for $x > 0.7$ over a progressively reduced range of asymmetries, the nuclear shapes at the ridge line are so profoundly necked-in that ridge and scission lines approximately coincide. This means that, as the system reaches a given point on the ridge line, it is, to a large extent, committed to decay with the corresponding saddle asymmetry. On the basis of the transition-state theory one can write, for the partial decay width:[21]

$$\Gamma(Z) = \frac{1}{2\pi\rho(E)} \int \rho^{**}[E - B(Z) - \epsilon]\, d\epsilon \qquad (5)$$

where $\rho(E)$ is the compound nucleus level density, and $\rho^{**}[E - B(Z) - \epsilon]$ is the level density at the conditional saddle of energy B(Z), which the system is transiting with kinetic energy ϵ.

Equation 5 can be further simplified as follows:

$$\Gamma_Z \propto \frac{\rho^{**}[E - B(Z)]}{\rho(E)} \propto e^{-B(Z)/T_Z} \qquad (6)$$

where T_Z represents the nuclear temperature calculated from the excitation energy above the barrier.
This means that the mass or charge yield mirrors the ridge line, being characterized by high emission probabilities in the regions of low potential energy and vice-versa. This is illustrated in Fig. 1 for two systems, one below the Businaro-Gallone point and the second above it. In the former case the yield has a characteristic U shape; in the latter case, one observes also a peak at symmetry which becomes more and more prominent with increasing fissility parameter x and which can be identified as the fission peak.

D. A transition state formalism for thermal spectra

In the case of neutron emission, the kinetic energy spectra can be easily calculated, since the velocity of the system at the conditional saddle corresponds closely to the velocity of the neutron at infinity. This is not quite the case for the emission of a charged complex fragment for which the kinetic energy at infinity comes also from the potential and kinetic energies associated with other modes.

We can write down the complex fragment decay rate in terms of the normal modes about a "saddle point" in a suitable deformation space.[20-21] It is helpful to consider a sphere-spheroid model where the smaller spherical fragment is in contact with a larger spheroidal fragment of variable eccentricity. The relevant collective degrees of freedom can be catalogued as shown in Fig. 3 in the framework of the sphere-spheroid model.

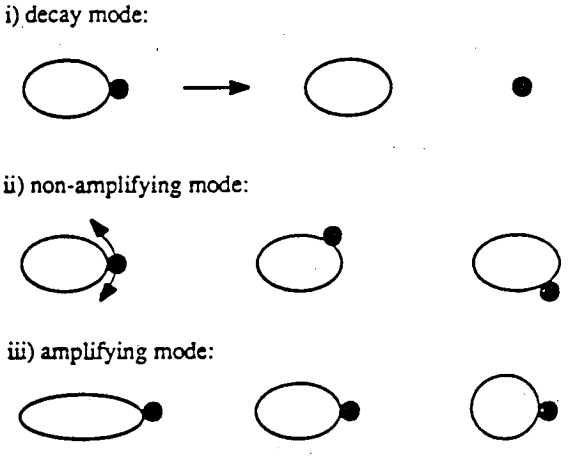

Fig. 3 Schematic representation of the three kinds of normal modes at the conditional saddle point, which control the kinetic energy at infinity.

The first class corresponds to the decay mode, which is unbound and analogous to the fission mode.

The second class includes the non-amplifying modes whose excitation energy is directly translated into kinetic energy at infinity without amplification. Two such modes could be, for instance, the two orthogonal oscillations of the particle about the tip of the "spheroidal" residual nucleus.

The third class corresponds to the amplifying modes. In these modes the total potential energy remains rather flat about the minimum, while complementary substantial changes occur in the Coulomb and surface energies. As shown in Fig. 4, an oscillation about this mode involving an amount of energy on the order of the temperature corresponds to a variation in the monopole - monopole term of the Coulomb energy

$$\Delta E_C = 2\sqrt{\frac{c^2 T}{k}} = 2\sqrt{pT} \qquad (7)$$

where the coefficients c and k are defined by the quadratic expansion of the total potential energy and by the linearization of the Coulomb energy along the deformation mode Z:

$$V(z) = B_0 + kz^2; \qquad E_{Coul} = E^0_{Coul} - cz. \qquad (8)$$

Because of its effect, illustrated in Fig. 4, p is called the "amplification parameter". An input thermal noise of the order of the temperature T is magnified in accordance to Eq. 7 and Fig. 4 giving an output kinetic energy fluctuation much greater than the temperature. This effect is probably responsible also for the great widths of the kinetic energy distributions in ordinary fission.

We are now going to consider two specific cases. The first and simplest deals in detail with only one decay mode and one amplifying mode. For this case the final kinetic energy distribution is:

$$P(E) = 1/2\,(\pi pT)^{1/2}\, e^{\frac{p}{4T}}\, e^{-\frac{x}{T}}$$

$$\left\{ \mathrm{erf}\left[\frac{2E^0_{Coul} + p}{2(pT)^{1/2}}\right] - \mathrm{erf}\left[\frac{p - 2x}{2(pT)^{1/2}}\right]\right\} \qquad (9)$$

where $x = E - E^0_{Coul}$.

The addition of <u>two</u> harmonic non-amplifying modes (potential energy only) like those illustrated in Fig. 3 or of <u>one</u> non-amplifying mode (potential + kinetic energy) leads to a more general expression:

$$P(E) = \frac{(\pi pT)^{1/2}}{2} e^{\frac{p}{4T}} e^{-\frac{x}{T}} \left[\frac{2x - p}{2} \left\{ \mathrm{erf}\left[\frac{2E^0 + p}{2(pT)^{1/2}}\right] - \mathrm{erf}\left[\frac{p - 2x}{2(pT)^{1/2}}\right]\right\} - \left(\frac{pT}{\pi}\right)^{1/2} \left\{ \exp - \left[\frac{(2E^0 + p)^2}{4pT}\right] - \exp - \left[\frac{(p - 2x)^2}{4pT}\right]\right\}\right] . \qquad (10)$$

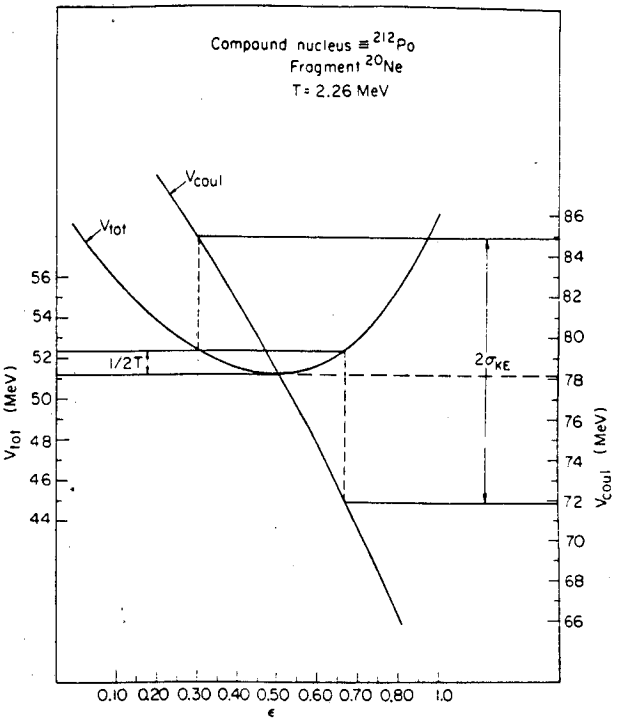

Fig. 4 Potential energy and Coulomb interaction energy as a function of the deformation of the large fragment (sphere-spheroid model). The thermal fluctuations about the ridge point result in larger amplified fluctuations in the Coulomb repulsion energy.[21]

This formula not only portrays the same features as that derived previously, but also allows for emission of the particle from any point of the surface (if the Coulomb potential is assumed to vary quadratically as the particle moves away from the pole toward the equator of the residual nucleus).

The general shapes predicted by these equations depend on the parameter p. At small values of p corresponding to the emission of small particles, the distributions are skewed and Maxwellian-like, while at larger values of p, corresponding to the emission of sizeable fragments, the distributions become Gaussians. This is illustrated in Figs. 5a & b, where the kinetic energy distributions assuming 0,1,2 non amplifying modes are calculated at various temperatures for the emission of an α particle (small p) and a carbon ion (large p) from a ^{212}Po compound nucleus.

In the limit of large p, these equations become of the form $p(x) \equiv \exp[-x^2/pT]$, which reminds us of the Gaussian kinetic energy distributions observed in ordinary fission. Another pleasing feature of these equations is the limit to which they tend for p=0:

$$P(E) \propto e^{-E/T} \quad \text{and} \quad P(E) \propto E\, e^{-E/T}. \qquad (11)$$

The latter form is the standard "evaporation" expression for the neutron spectra. Therefore the evolution of the kinetic energy spectra from Maxwellian-like to Gaussian-like as one goes from "evaporation" to "fission" is naturally predicted in this model.

E. Angular distributions

Continuing the generalization of the fission process, the angular distributions for the emitted particles can also be derived. The ridge-point configuration, for the great majority of cases, can be identified with the scission configuration. Furthermore, the disintegration axis and the symmetry axis of the system at the ridge point should approximately coincide. As a consequence, the projection K of the total angular momentum I on the symmetry/disintegration axis should remain constant from the ridge point to infinity. In the present case, the closeness of the ridge and the scission points should make the theory work even better than in fission.

Then the angular distribution becomes:[21]

$$W(\theta) \propto \exp(-s_{max})\left[I_0(s_{max}) + I_1(s_{max})\right] + \frac{\beta I^2_{max}}{2}\exp(-s_{max})\left[I_0(s_{max}) + \frac{2I_1(s_{max})}{3} - \frac{I_2(s_{max})}{3}\right] \qquad (12)$$

where $s_{max} = I^2_{max}\sin^2\theta/4K^2_o$, and I_o, I_1, I_2 are the modified Bessel functions of order 0, 1,2. This expression has two interesting limits. As $g = I^2_{max}/4K^2_o$ tends to infinity (either because K^2_o tends to zero or because I_{max}

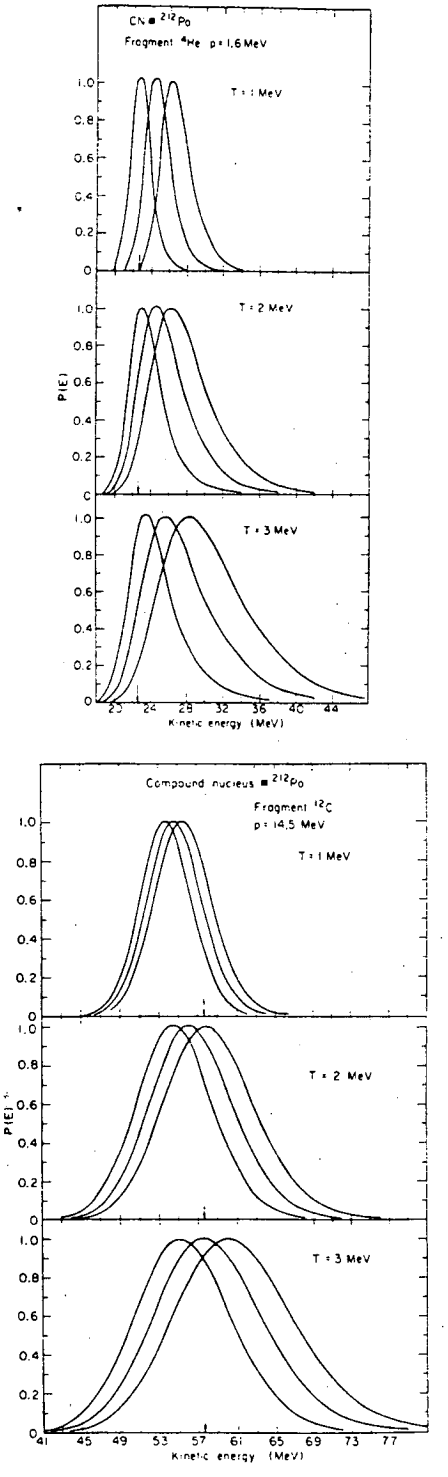

Fig. 5 Calculated kinetic energy distributions at three temperatures for small [(a) α particles] and large [(b)^{12}C fragments] values of the amplification parameter p for the decay of a ^{212}Po nucleus. The curves corresponding to 0,1,2 non amplifying modes can be identified by their progressive shift towards higher kinetic energies. The arrows indicate the energies corresponding to the ridge line Coulomb energies.[21]

becomes very large), one obtains:

$$\lim_{g \to \infty} \quad W(\theta) \propto \frac{1}{\sin \theta} . \qquad (13)$$

On the other hand, as $g \to 0$ (either because $I_{max} \approx 0$ or $K^2_o \to \infty$) one obtains:

$$\lim_{g \to 0} \quad W(\theta) = \text{constant} . \qquad (14)$$

These limits represent the two extreme cases for the coupling between total and orbital angular momentum. The coupling parameter g depends upon the principal moments of inertial of the ridge configuration. This allows one to make a very simple prediction. At constant I_{max}, g becomes larger the bigger the difference between $\Im_{||}$ and $\Im_{\perp}$, or in other words, the more elongated the ridge configuration is. Thus the anisotropy $W(0^0)/W(90^0)$ progressively increases as one considers the emission of a neutron, an α-particle, a lithium particle, a beryllium particle, etc. (see Fig. 6).

III. EXPERIMENTAL EVIDENCE FOR STATISTICAL BINARY DECAY

A. Compound nucleus emission at low energies

In the midst of a confusing experimental situation at intermediate energies, a descent to lower energies helped to clarify the compound nucleus emission of complex fragments. The reaction chosen for this purpose,[35] was ^{3}He + Ag. The excitation energy of the compound nucleus ranged from 50 MeV to 130 MeV, the lower limit being barely 10 MeV above the highest barriers. Complex fragments were detected with cross sections dropping precipitously with decreasing energy. Their kinetic energy spectra resembled closely the shapes predicted by the theory illustrated above. In particular, the shapes evolved from Maxwellian-like for the lowest Z values to Gaussian-like for the highest Z values.

However, the crucial proof is given by the measurement of excitation functions extending down almost to the threshold. These excitation functions, are shown in Fig. 7. They demonstrate with their rapid rise with increasing energy, that these fragments originate from compound nucleus decay and compete, in their emission, with the major decay channel, namely neutron emission.

The compound nucleus fits shown in the same figure, on the one hand demonstrate quantitatively the agreement with the compound nucleus hypothesis, and on the other allow one to extract the conditional barriers. The extracted barriers are presented in Fig. 8 together with two calculations.[25] The standard liquid-drop model fails dramatically in reproducing the barriers, while the finite-range model, accounting for the surface-surface interaction (so important for these highly indented conditional saddle shapes) reproduces the experimental values almost exactly.

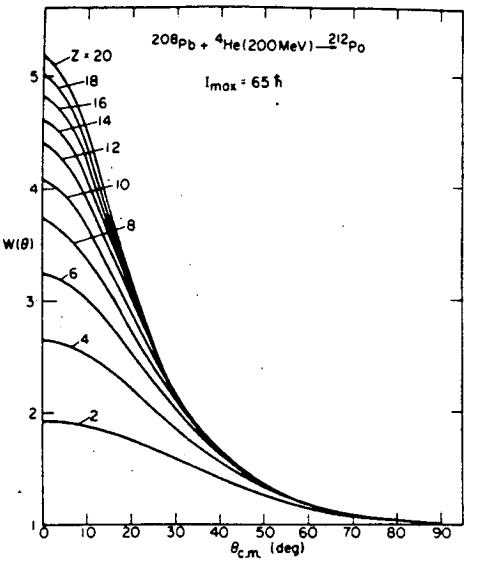

Fig. 6 Calculated angular distributions of various fragments emitted by the compound nucleus formed in the reaction ^{208}Pb + 200 MeV ^{4}He $\rightarrow$ [^{212}Po*] $\rightarrow$ Z + (84 - Z). Note the progressive approach to a 1/sin θ distribution with increasing atomic number of the fragments.[21]

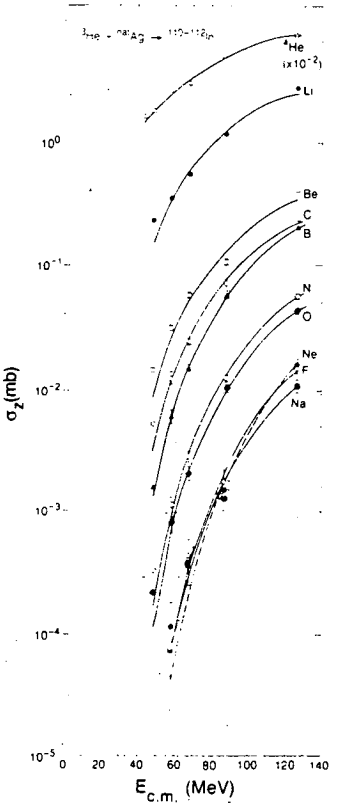

Fig. 7 Dependence of the total integrated cross sections (symbols) for emission of complex fragments on the center-of-mass energy, $E_{c.m.}$, in the reaction ^{3}He + ^{nat}Ag. The curves are compound nucleus fits to the data.[44]

Additional studies at low energies have demonstrated the role of the potential energy along the ridge line.[36] As was shown previously, the charge distribution is U shaped or has an additional maximum at symmetry depending on whether the system is below or above the Businaro-Gallone point. The three reactions $^{74}Ge + {}^{9}Be$, $^{93}Nb + {}^{9}Be$ and $^{139}La + {}^{9}Be$, studied at 8.5 MeV/u, produce compound nuclei well below, near, and well above the Businaro-Gallone point, respectively. The observed fragments were emitted from a source with compound nucleus velocity and were characterized by center-of-mass Coulomb-like energies. Their charge distributions are shown in Fig. 9 together with the corresponding compound nucleus calculations. As expected, the U-shaped distributions prevailing at or below the Businaro-Gallone point as exemplified by the $^{74}Ge + {}^{9}Be$ and $^{93}Nb + {}^{9}Be$ reactions, develop in the case of $^{139}La + {}^{9}Be$ a central peak, characteristic of systems above the Businaro-Gallone point. The solid curves in the same figure represent calculations based on the compound nucleus hypothesis.

B. Compound nucleus emission at higher energies

Compound nucleus emission of complex fragments at low energy implies an even more abundant emission at higher energies, provided that compound nuclei are indeed formed. Part of the initial confusion about complex fragment emission at intermediate energies may have been due to the broad range of compound and non compound nucleus sources associated with the onset and establishment of incomplete fusion. This problem can be minimized to some extent by the choice of rather asymmetric systems. In such systems, the range of impact parameters is geometrically limited by the nuclear sizes of the reaction partners. Furthermore, the projectile-like spectator, if any, is confined to very small masses, and does not obscure other sources of complex fragments.

Incomplete fusion or massive transfer appears to begin at approximately 18 MeV/N bombarding energy and extends probably higher than 100 MeV/u. At even higher bombarding energies, it may be replaced by a participant-spectator mechanism in which the interacting nucleons form a fireball physically separated from the rather cool spectators.

Many reactions have been studied in reverse kinematics to facilitate the detection of most of the fragments over a large center-of-mass angular range.

Representative examples[37] of the invariant cross sections in the $v_{\parallel}$ - $v_{\perp}$ plane for a range of atomic numbers are shown in Fig. 10. For all the reactions studied so far, one observes beautifully developed Coulomb rings whose isotropy indicate that, up to 50 MeV/u, the fragments do in fact arise from binary compound nucleus decay.[37-39] Only the fragments in the neighborhood of the target atomic number show the presence of an additional component at backward angles (big foot), that can be attributed to quasi-elastic and deep-inelastic processes, and/or to the spectator target-like fragment in the incomplete-fusion reactions prevailing at higher bombarding energies.

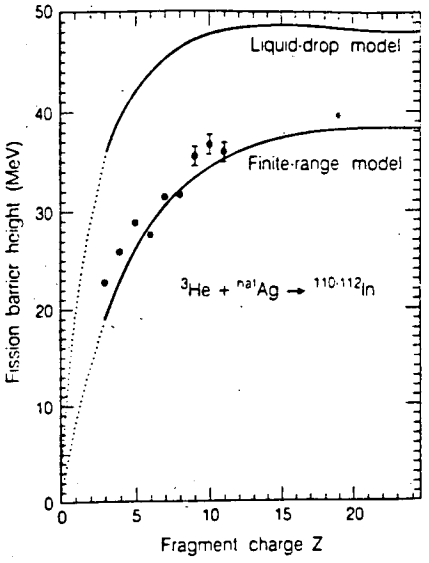

Fig. 8 Calculated[25] and experimental[44] conditional fission barriers as a function of the lighter fragment charge for the fission of ^{111}In. The experimental values are obtained from the fits in Fig. 7. The calculated curves for the liquid drop and finite-range models are shown. The dotted portions of the curves are extrapolations.

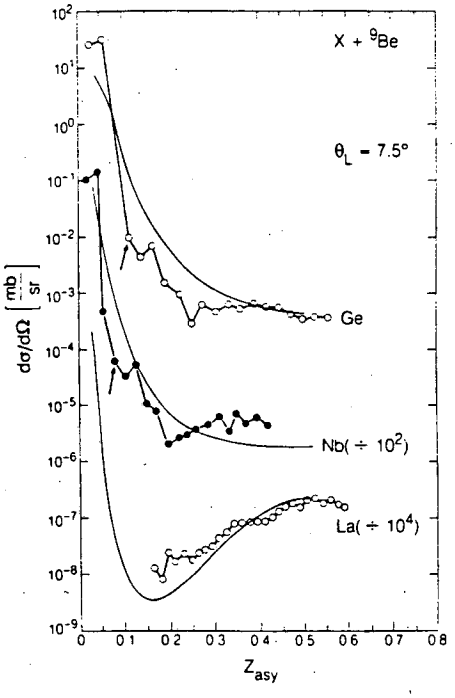

Fig. 9 Center-of mass cross sections[36] for products from the 8.5 MeV/u ^{74}Ge, ^{93}Nb, $^{139}La + {}^{9}Be$ systems detected at $\theta_{lab} = 7.5^{o}$. The solid line is a compound nucleus calculation of the fragment yield at $\theta_{c.m.} = 30^{o}$. The arrows indicate the entrance-channel asymmetry.

The center of each ring provides the source velocity for each Z value. For all bombarding energies the extracted source velocities are independent of the fragments' Z value. Up to ~18 MeV/u, one can conclude that a single source with compound nucleus velocity is responsible for the emission of all the fragments. As the bombarding energy increases, it appears that incomplete fusion sets in. The observed source velocities are intermediate between the projectile and compound nucleus velocities. In the case of 50 MeV/u ^{139}La + ^{12}C, the source velocity is halfway between the two limits, indicating that ~1/2 of the ^{12}C target fuses with the ^{139}La projectile.[39] It is truly remarkable that even when incomplete fusion sets in, the source velocity is independent of Z value and quite sharp.

The radii of the Coulomb rings give the emission velocities in the center of mass. The almost linear dependence of these velocities upon fragment Z value is a clear indication of their Coulomb origin. This is also supported by their independence of bombarding energy.[38] The Coulomb calculations reproduce the data, further illustrating the degree of relaxation of the c.m. kinetic energy. The variances of the velocities arise from a variety of causes, among which the inherent Coulomb energy fluctuation due to the shape fluctuations of the "scission point", and the fragment recoil due to sequential evaporation of light particles.

C. Cross sections

All of the evidence presented so far for the intermediate energy complex fragment emission points rather convincingly towards a compound nucleus process. However, the most compelling evidence for this compound mechanism lies in the statistical competition between complex fragment emission and the major decay channels, like n, p, and ^{4}He emission. The simplest and most direct quantity testing this hypothesis is the absolute cross section.

Absolute cross sections as a function of Z value are shown in Figs. 11-15. At first glance one can observe a qualitative difference between the charge distributions from the ^{93}Nb-induced and the ^{139}La-induced reactions. The former distributions portray a broad minimum at symmetry whereas the latter show a broad central fission-like peak that is absent in the former distributions. This difference can be traced to the fact that the former systems are below or near the Businaro-Gallone point while the latter systems are well above.

In general, for a given system, the cross sections associated with the charge distributions increase in magnitude rapidly at low energies, and very slowly at high energy, in a manner consistent with Eq. 6.

The most important information associated with these cross sections is their absolute value and energy dependence. Through them, the competition of complex fragment emission with the major decay channels, like n, p, and a decay is manifested. This is why we attribute a great deal of significance to the ability to fit such data. Examples of these fits are shown in Figs. 11-15. The calculations are performed with an evaporation code GEMINI[38] extended to

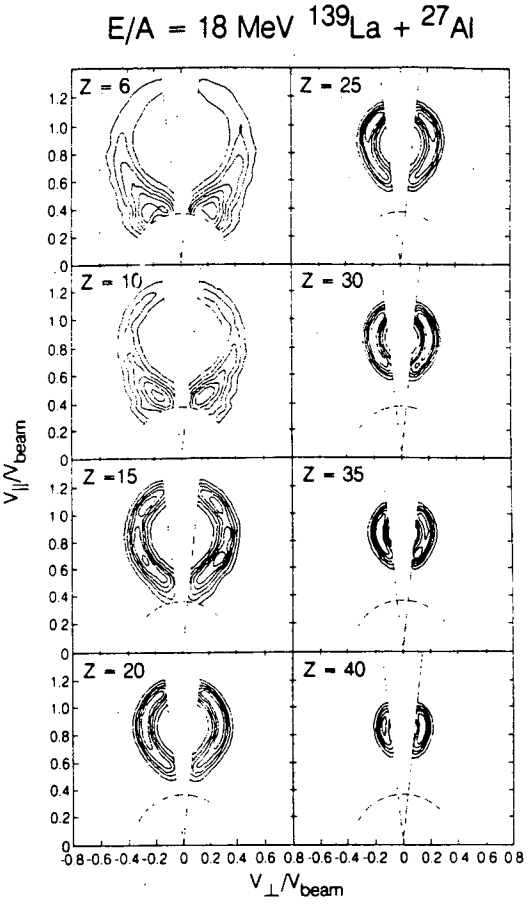

Fig. 10 Contours of the experimental cross section $\partial^2\sigma/\partial V_{||}\partial V_{\perp}$ in the $V_{||}$-$V_{\perp}$ plane for representative fragments detected in the reaction E/A = 18 MeV ^{139}La + ^{12}C. The beam direction is vertical towards the top of the figure. The dashed lines show the maximum and minimum angular thresholds and the low velocity threshold of the detectors. The magnitudes of the contour levels indicated are relative.[37]

incorporate complex fragment emission. Angular momentum dependent finite-range barriers are used.[25] All the fragments produced are allowed to decay in turn both by light particle emission or by complex fragment emission. In this way higher chance emission, as well as sequential binary emission, are accounted for.

The cross section is integrated over ℓ waves up to a maximum value that provides the best fit to the experimental charge distributions. In the case of the ^{93}Nb + ^{9}Be & ^{12}C, as well ^{139}La + ^{12}C for bombarding energies up to 18 MeV/u, the quality of the fits is exceptionally good and the fitted values of ℓ_{max} correspond very closely to those predicted by the Bass model[40] or by the extra push model,[41] as shown in Fig. 16.

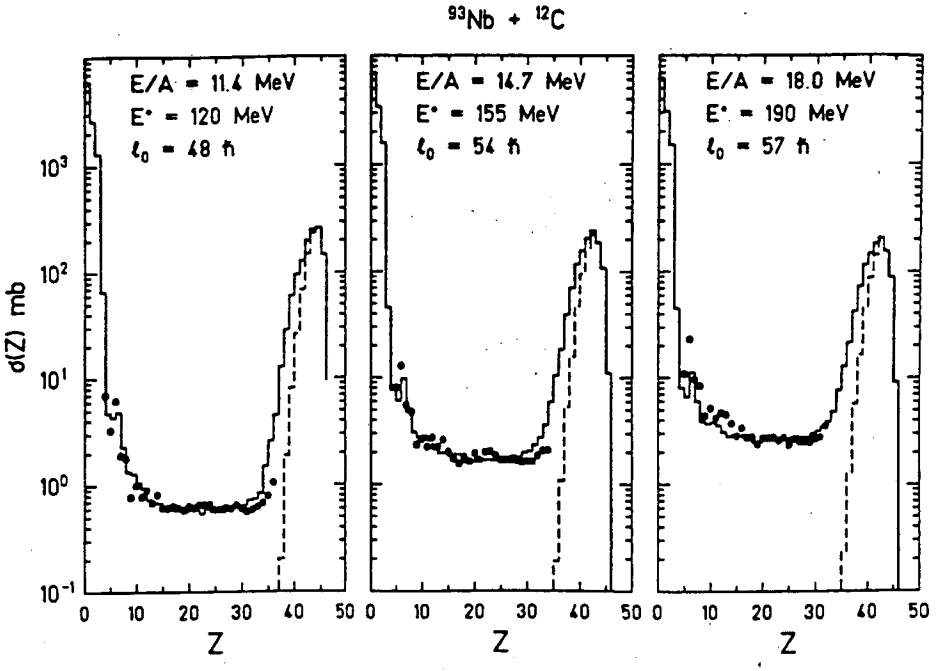

Fig. 11 Angle-integrated charge distributions (solid circles) of complex fragments associated with fusion-like reactions of ^{93}Nb and ^{12}C at three bombarding energies.[38] The histograms represent calculations with the statistical code GEMINI.[45]

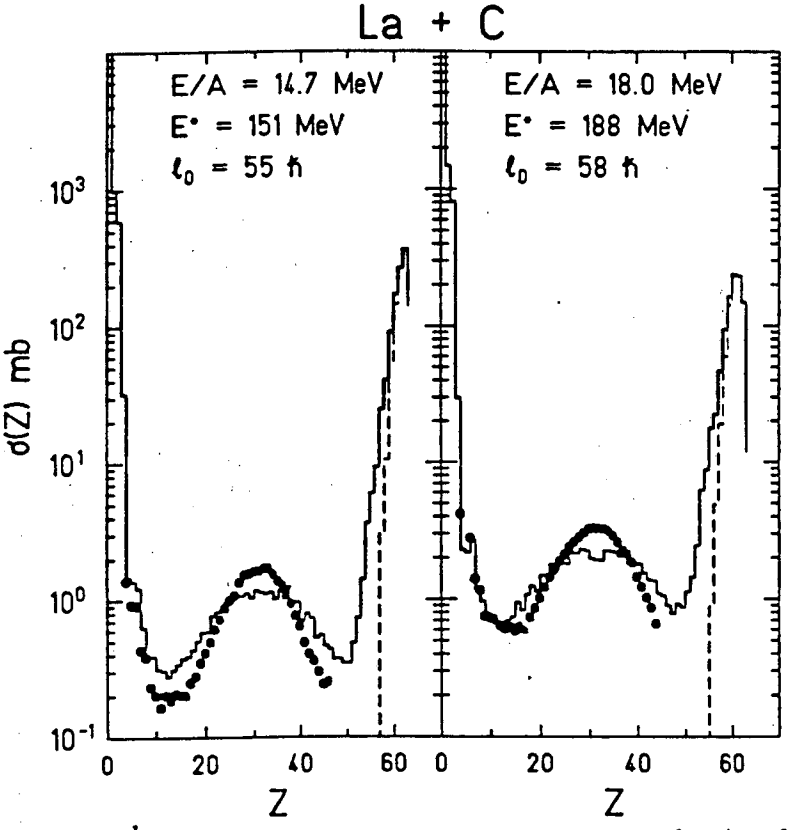

Fig. 12 Angle-integrated cross sections (solid circles) plotted as a function of the fragment Z-value for the 14 & 18 MeV/u ^{139}La + ^{12}C reactions.[37] The histograms represent calculations with the statistical code GEMINI.[38]

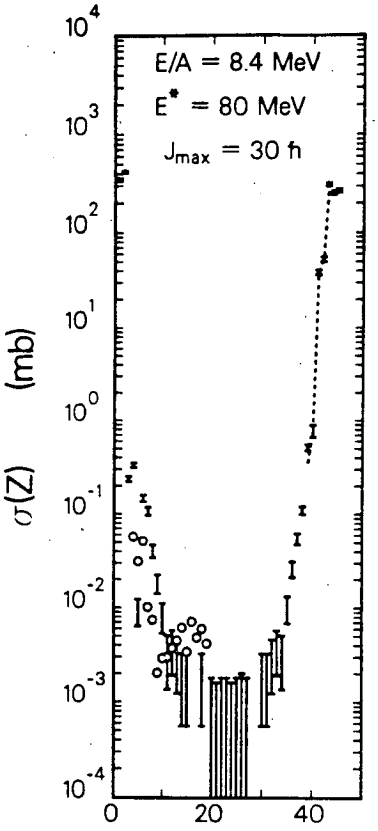

Fig. 13 Comparison of experimental and calculated charge distributions for the ^{93}Nb + ^{9}Be reaction at 8.5 MeV/u. The experimental data are indicated by the hollow circles and the values calculated with the code GEMINI are shown by the error bars.[38] The dashed curve indicates the cross sections associated with classical evaporation residues which decay only by the emission of light particles ($Z \leq 2$). Note the value of the excitation energy (E^*) corresponding to complete fusion and the value of J_{max} assumed to fit the data.

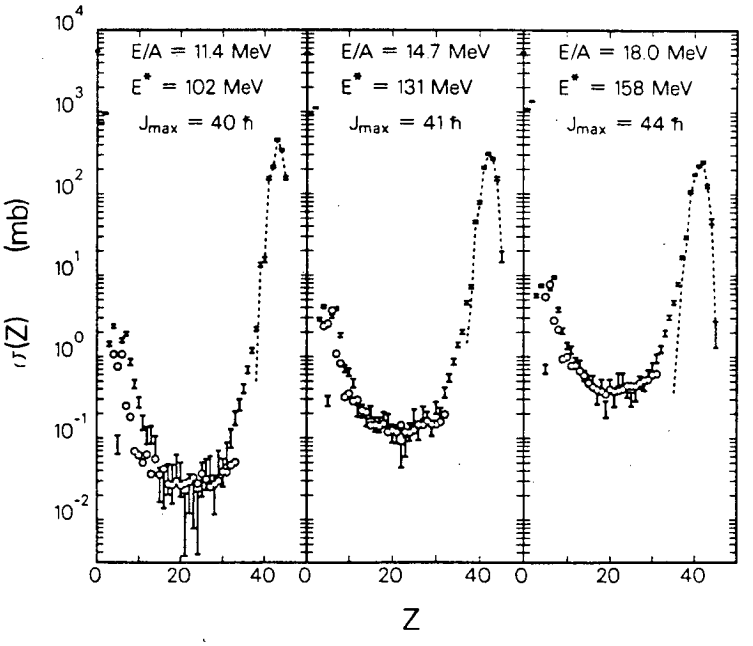

Fig. 14 Comparison of experimental and calculated charge distributions for the ^{93}Nb + ^{9}Be reaction at E/A = 11.4, 14.7, and 18.0. See Fig. 13.

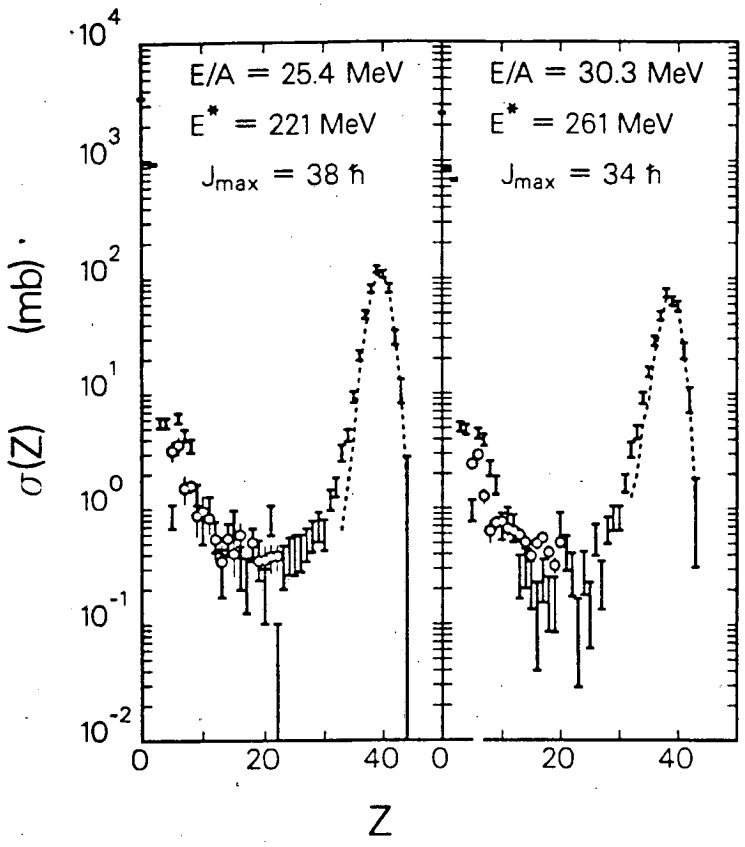

Fig. 15 Same as in Fig. 14, for the ^{93}Nb + ^{9}Be reaction[46] at E/A =25.4 and 30.3.

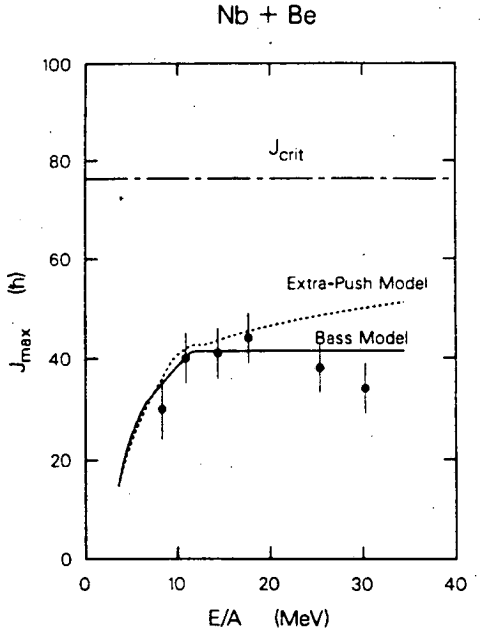

Fig. 16 Plot showing the maximum angular momentum for fusion (J_{max}) obtained by fitting the experimental charge distributions as a function of bombarding energy for the ^{93}Nb + ^{9}Be reactions. The dashed and solid curve show the predictions of the extra-push and Bass models, respectively. The chain dashed lines indicate the angular momentum (J_{crit}) where the barrier for symmetric division vanishes.[38]

D. Coincidence data

If any doubt still remains concerning the binary nature of the decay involved in complex fragment production, it can be removed by the detection of binary coincidences. Several examples of Z_1 - Z_2 correlations are shown in Figs. 17 & 18. Some examples of the sum (Z_1 + Z_2) spectra are also shown in Figs. 19 & 20. One can observe the binary band in the Z_1 - Z_2 correlation as a general feature persisting up to the highest bombarding energies (100 MeV/u for ^{139}La + ^{12}C)! The binary nature is proven by the correlation angles as well as by the sum of the fragments' atomic numbers which accounts for most of the target + projectile charge. The missing charge can be accounted for by the extent of incomplete fusion and by the sequential evaporation of light charged particles ($A \leq 4$). A particularly interesting example of this verification is shown in Fig. 21 for the reactions ^{93}Nb + ^{9}Be, ^{27}Al. In this figure, the average charge sum Z_1 + Z_2 is shown as a function of Z_2. The dashed lines indicate the charge of the compound nucleus obtained in an incomplete fusion process as calculated from the measured source velocities. The solid lines show the reduction in charge brought about by evaporation from the hot primary fragments formed in the binary decay. The excitation energy of the fragments was evaluated on the basis of the source velocity, which tells about the extent of incomplete fusion. The remarkable agreement of these calculations with the data, which is retained over a large range of excitation energies speaks for the internal consistency of such an analysis.

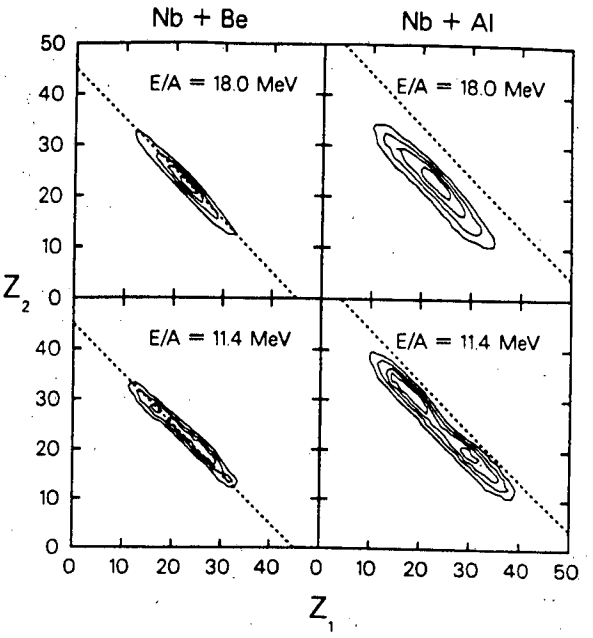

Fig. 17 Representative Z_1-Z_2 contour plots for coincidence events from the reactions ^{93}Nb + ^{9}Be & ^{27}Al at 11.4 and 18.0 MeV/u. Z_1 and Z_2 refer to the Z-values of fragments detected in two detectors at equal angles on opposite sides of the beam .[38]

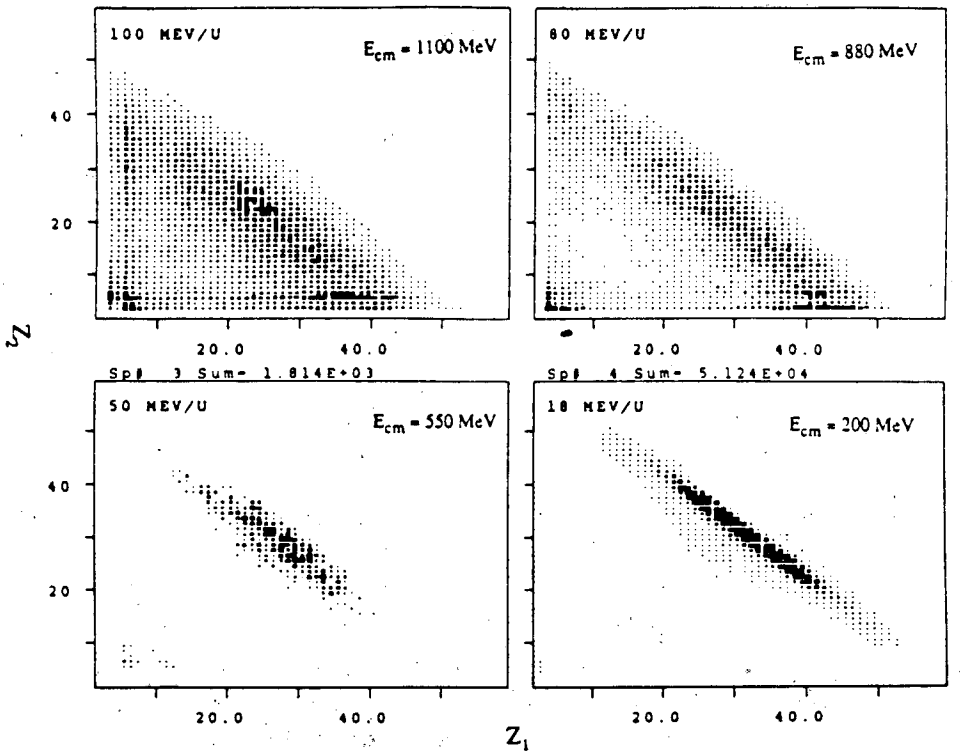

Fig. 18 Scatter plots of the experimental Z_1 - Z_2 correlation for coincident fragments detected at symmetric angles on opposite sides of the beam in the ^{139}La + ^{12}C reactions at 18, 50, 80, and 100 MeV/u.[37,39,47]

This same consistency holds over a very wide range of bombarding energies (8.5 - 30.3 MeV/u). In Fig. 22 the average sum of the symmetric products' final atomic numbers for the reaction $^{93}Nb + ^{27}Al$ is plotted vs bombarding energy. The five experimental points correspond to bombarding energies of 11.4, 14.7, 18, 25.4 and 30.3 MeV/u. The solid line represents the sum of the target and projectile atomic numbers. The long dashed line corresponds to the compound nucleus atomic number calculated on the basis of the momentum transfer systematics[42] in incomplete fusion. The short dashed line corresponds to the sum of the charges of the final fragments after evaporation as calculated with the code PACE.[43] The agreement between calculation and experiment is very satisfactory and supports our basic understanding of incomplete fusion, mass and energy transfer, as well as of sequential evaporation.

Finally, it is possible to verify that the coincidence rate and the single rate are consistent with each other under the assumption that all the fragments arise from binary decay. This can be done by evaluating the experimental coincidences/singles ratio on one hand, and on the other by computing the same ratio from the singles rate and from the knowledge of the efficiencies of the detectors involved in the coincidence measurement. The good agreement which is observed indicates that all of the coincidences can be accounted for by the singles data. In other words, all the singles data are associated with binary processes.

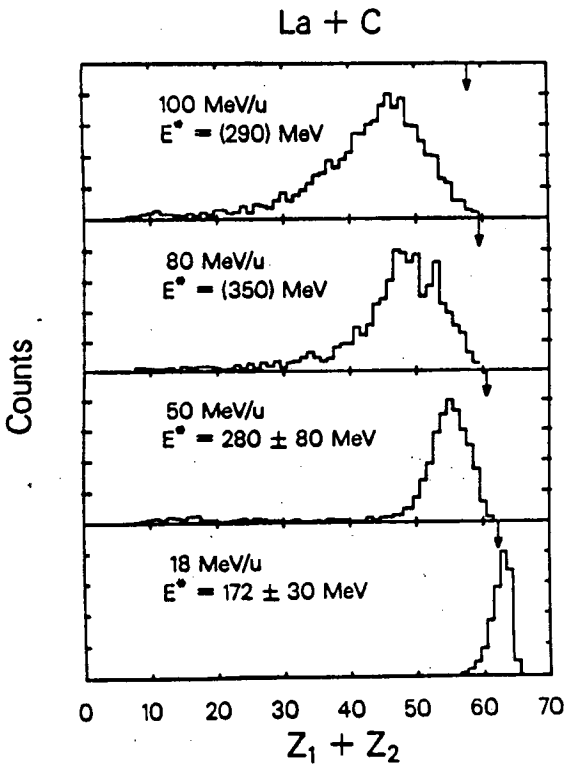

Fig. 20 The relative yield of coincidence events plotted as a function of the sum of the atomic charges of the two coincident fragments for the $^{139}La + ^{12}C$ reactions at 18, 50, 80 and 100 MeV/u.

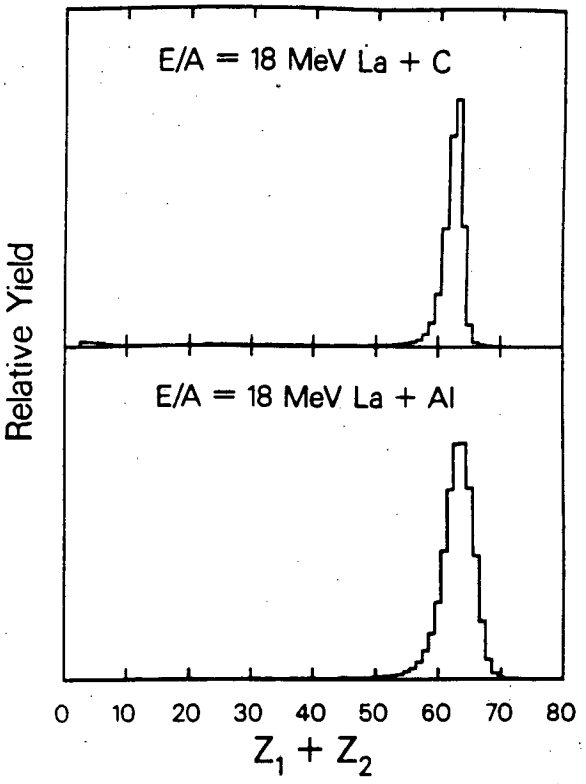

Fig. 19 The relative yield of coincidence events plotted as a function of the sum of the atomic charges of the two coincident fragments for the $^{139}La + ^{12}C$ & ^{27}Al reactions at 18 MeV/u.[37]

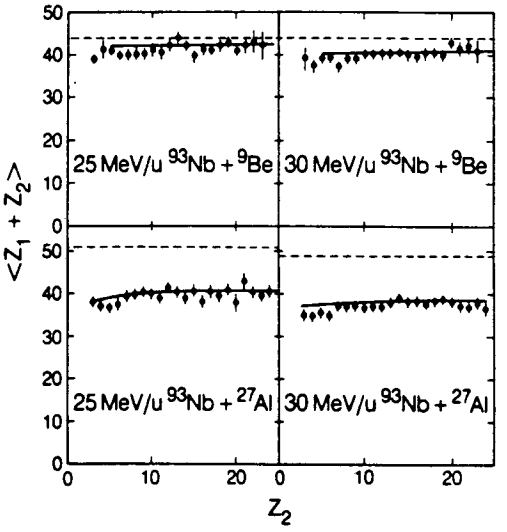

Fig. 21 The mean sum, $\langle Z_1 + Z_2 \rangle$ of coincidence events plotted as a function of Z_2 for the $^{93}Nb + ^{9}Be$ & ^{27}Al reactions at 25.4 and 30.3 MeV/u. The dashed lines indicate the average charge of the source system estimated from the mass transfer. The charge loss for binary events due to sequential evaporation was estimated using the evaporation code PACE, and the residual $Z_1 + Z_2$ values are indicated by the solid curves.[46]

IV. OUTLOOK AND CONCLUSIONS

The explicit treatment of the mass asymmetry degree of freedom has allowed us to extend the concept of fission to statistical processes involving the emission of fragments of any size. This generalization makes fission a process that extends throughout the periodic chart and that incorporates as special cases both traditional fission and light particle evaporation.

The experimental evidence allows us to conclude that the statistical emission of complex fragments as a generalized fission process is well established, and its role has been proven important from the lowest excitation energies up to the limits of compound nucleus stability.

Despite the extensive research covered in this presentation, a lot if not most of the work remains yet to be done. The experimental determination of the conditional barriers is so far limited to one isotope, and even that is incomplete. A systematic study of the conditional barriers is clearly necessary to test the validity (or to define the parameters) of the macroscopic models like the finite range model. As it has been done for the symmetric barriers in heavy systems, it should be possible to isolate the shell effects from the macroscopic part of the conditional barriers. Furthermore, the knowledge of the conditional barriers is essential for the predictions of cross sections and reaction rates.

A natural development of these studies should lead to the evaluation of the dependence of the barriers upon angular momentum on one hand and upon temperature on the other. It may well be that complex fragment emission will be the most powerful if not the only tool for the characterization of extremely hot nuclei, their free energy and the temperature dependence of the coefficients of its liquid drop-like expansion. As we are writing, the role and scope of intermediate energy nuclear physics is being debated and defined in the experimental and theoretical arenas. If intermediate energy nuclear physics is the physics of hot nuclei near the limit of their (thermal) stability, it is clear already that fission in its generalized aspect of complex fragment emission will be a shining beacon in the golden twilight of nuclei.

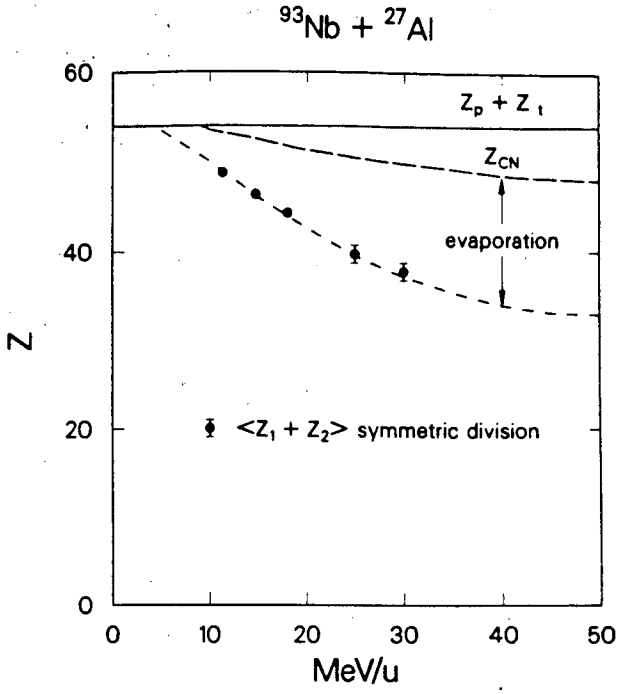

Fig. 22 Comparision of the experimentally determined sum of the charges for symmetric products with calculations performed on the basis of incomplete fusion and sequential evaporation from the primary binary fragments. Data points are shown for five bombarding energies for the $^{93}Nb + ^{27}Al$ reaction.

ACKNOWLEDGEMENTS

This work was supported by the Director, Office of Energy Research, Office of High Energy and Nuclear Physics, Division of Nuclear Physics of the U. S. Department of Energy under Contract DE-AC03-76SF00098.

REFERENCES

1. J. M. ALEXANDER, C. BALTZINGER, and M. F. GAZDIK, Phys.Rev., 129, 1826 (1963).
2. A. A. CARETTO, J. HUDIS, and G. FRIEDLANDER, Phys. Rev., 110, 1130 (1958).
3. G. FRIEDLANDER, J. M. MILLER, R. WOLFGANG, J. HUDIS, and E. BAKER, Phys. Rev., 94, 727 (1954).
4. G. FRIEDLANDER, L. FRIEDMAN, B. GORDON, and YAFFE, Phys. Rev., 129, 1809 (1963).
5. W. U. SCHRÖDER, and J. R. HUIZENGA, Ann. Rev. Nucl. Part. Sci., 27, 465 (1977).
6. L. G. MORETTO and R. P. SCHMITT, J. Phys., 37C5 109 (1976).
7. L. G. MORETTO and G. J. WOZNIAK, Ann. Rev. Nucl. Part. Sci., 34, 189 (1984).
8. J. AICHELIN and J. HÜFNER, Phys. Lett., 138B, 15 (1984).
9. M. E. FISCHER, Phys., 3, 255 (1967).
10. M. E. FISCHER, Rep. Prog. Phys., 67, Vol. 30 615 (1967).
11. G. SAUER, H. CHANDRA, and U. MOSEL, Nucl. Phys., A264, 221 (1976).
12. J. E. FINN, S. AGARWAL, A. BUJAK, J. CHUANG, L. J. GUTAY, A. S. HIRSCH, R. W.

MINICH, N. T. PORILE, R. P. SCHARENBERG, B. C. STRINGFELLOW, and F. TURKOT, Phys. Rev. Lett., 49, 1321 (1982).

13. G. BERTSCH and P. J. SIEMENS, Phys. Lett., 126, 9 (1983).

14. P. J. SIEMENS, Nature , 395, 410 (1983).

15. V. F. WEISSKOPF, Phys. Rev., 52, 295 (1937).

16. V. F. WEISSKOPF and D. H. EWING, Phys. Rev., 57 472 (1940).

17. V. F. WEISSKOPF, Phys. Acta , 23, 187 (1950).

18. V. F. WEISSKOPF, Arts Sci., 82, 360 (1953).

19. J. A. WHEELER, Fast neutron physics part II, Interscience, New York, pp. 2051 (1963).

20. L. G. MORETTO, Phys. Lett., 40B, 185 (1972).

21. L. G. MORETTO, Nucl. Phys., A247, 211 (1975).

22. S. COHEN, F. PLASIL, and W. J. SWIATECKI, Proc. Third Conf. on Reactions Between Complex Nuclei, ed. A. Ghiorso, R. M. Diamond and H. E. Conzett (University of California Press) pp. 325 UCRL-10775 (1963).

23. S. COHEN, F. PLASIL, and W. J. SWIATECKI, Ann. Phys., 82, 557 (1974).

24. J. R. NIX and W. J. SWIATECKI, Nucl. Phys., 71, 1 (1965).

25. A. J. SIERK, Phys. Rev. Lett., 55, 582 (1985).

26. A. J. SIERK, Phys. Rev., C33, 2039 (1986).

27. U. L. BUSINARO and S. GALLONE, Nuovo Cimento, 1, 1277 (1955).

28. S. W. BARWICK, P. B. PRICE, H. L. RAVN, E. HOURANI, and H. HUSSONNOIS, Phys. Rev., C34, 362 (1986).

29. S. GALES, E. HOURANI, M. HUSSONNOIS, J. P. SCHAPIRA, L. STAB, and M. VERGNES, Phys. Rev. Lett., 53, 759 (1984).

30. P. B. PRICE, J. D. STEVENSON, S. W. BARWICK, and H. L. RARN, Phys. Rev. Lett., 54, 297 (1985).

31. H. J. ROSE and G. A. JONES, Nature, 307, 245 (1984).

32. D. N. POENARU, M. IVASCU, A. SANDULESCU, and W. GREINER, Phys. Rev., C32, 572 (1985).

33. Y. J. SHI and W. J. SWIATECKI, Phys. Rev. Lett., 54, 300 (1985).

34. Y. J. SHI and W. J. SWIATECKI, Nucl. Phys., A438, 450 (1985).

35. L. G. SOBOTKA, M. L. PADGETT, G. J. WOZNIAK, G. GUARINO, A. J. PACHECO, L. G. MORETTO, Y. CHAN, R. G. STOKSTAD, I. TSERRUYA, and S. WALD, Phys. Rev., Lett. 51, 2187 (1983).

36. L. G. SOBOTKA, M. A. McMAHAN, R. J. McDONALD, C. SIGNARBIEUX, G. J. WOZNIAK, M. L. PADGETT, J. H. GU, Z. H. LIU, Z. Q. YAO, and L. G. MORETTO, Phys. Rev. Lett., 53, 2004 (1984).

37. R. J. CHARITY, N. COLONNA, M. A. McMAHAN, G. J. WOZNIAK, R. J. McDONALD, L. G. MORETTO, G. GUARINO, A. PANTALEO, L. FIORE, A. GOBBI, and K. D. HILDENBRAND, Lawrence Berkeley Laboratory preprint, LBL-26859 (1989).

38. R. J. CHARITY, M. A. McMAHAN, G. J. WOZNIAK, R. J. McDONALD, L. G. MORETTO, D. G. SARANTITES, L. G. SOBOTKA, G. GUARINO, A. PANTALEO, L. FIORE, A. GOBBI, and K. D. HILDENBRAND, Nucl. Phys., A483, 371 (1988).

39. D. R. BOWMAN, W. L. KEHOE, R. J. CHARITY, M. A. McMAHAN, A. MORONI, A. BRACCO, S. BRADLEY, I. IORI, R. J. McDONALD, A. C. MIGNEREY, L. G. MORETTO, M. N. NAMBOODIRI, and G. J. WOZNIAK, Phys. Lett., B189, 282 (1987).

40. R. BASS, Nucl. Phys., A231, 45 (1974).

41. W. J. SWIATECKI, Nucl. Phys., A376, 275 (1982).

42. V. E. VIOLA, B. B. BACK, K. L. WOLF, T. C. AWES, C. K. GELBKE, and H. BREUER, Phys. Rev., C26, 178 (1982).

43. A. GAVRON, Phys. Rev., C21, 230 (1980).

44. M. A. McMAHAN, L. G. MORETTO, M. L. PADGETT, G. J. WOZNIAK, L. G. SOBOTKA, and M. G. MUSTAFA, Phys. Rev., Lett. 54, 1995 (1985).

45. R. J. CHARITY, private communication.

46. R. J. CHARITY, D. R. BOWMAN, Z. H. LIU, R. J. McMDONALD, M. A. McMAHAN, G. J. WOZNIAK, L. G. MORETTO, S. BRADLEY, W. L. KEHOE, and A. C. MIGNEREY, Nucl. Phys., A476, 516 (1988).

47. D. R. BOWMAN, G. F. PEASLEE, N. COLONNA, M.A. McMAHAN, H. HAN, K. JING, D. DELIS, G. J. WOZNIAK, L. G. MORETTO, W. L. KEHOE, B. LIBBY, A. MARCHETTI, A. C. MIGNEREY, A. MORONI, S. ANGIUS, A. PANTELEO, AND G. GUARINO, LBL-2688, (1989).

LAWRENCE BERKELEY LABORATORY
TECHNICAL INFORMATION DEPARTMENT
1 CYCLOTRON ROAD
BERKELEY, CALIFORNIA 94720